Vinogradov V, Knyazhansky M, Tsun A. Experimental observation and numerical modeling of formation of local plastic zones in hardened surface layers due to contact overloading. Mechanics of Materials 2015, 83, 90–102.

Experimental observation and numerical modeling of formation of local plastic zones in hardened surface layers due to contact overloading

V. Vinogradov [a*], M. Knyazhansky [b], A.Tsun[c]

[a] School of Civil Engineering and Geosiences, Newcastle University, Newcastle upon Tyne, NE1 7RU, U.K.

[b] Department of Software Engineering, Shamoon College of Engineering, Beer-Sheva, 84100, Israel

[c] Raymond and Beverly Sackler Faculty of Exact Sciences, School of Physics and Astronomy, Tel-Aviv University, Tel-Aviv, 69978, Israel

Abstract

The problem of formation of plastic zones in case-hardened metallic bodies due to contact overloading is studied both experimentally and numerically. Metallic materials exposed to surface hardening demonstrate a spatial variation of the material hardness and yield strength with a decreasing profile with depth and belong to the class of so-called plastically graded materials. The presented experimental program employs micro-Vickers hardness tests to map the variation in material hardness and corresponding yield strength for both virgin and loaded case-hardened specimens made of a chromium tool steel. It is shown that, depending on the profile of the yield strength in the near-surface zones and contact parameters, a plastic deformation can originate underneath the hardened layer. The distribution of the effective plastic strain extracted from the micro-hardness increment measurements are found in good agreement with the results of finite element simulations of a plastically graded material subjected to similar loading conditions. Numerical analysis reveals significant perturbations in the stress field distribution within the hardened layer due to formation of a closed-shaped plastic zone in the gradient layers, including development of a tensile stress on the boundary between the elastic and plastic zones as well as an overall increase in the effective stress intensity. It is shown that the hardened layer behaves similar to an elastic beam on a compliant foundation. These stress field perturbations in the hardened layers with low deformation capacity can greatly affect the durability and serviceability of surface treated mechanical parts.

Keywords: Case hardening, Plastically graded materials, Plastic zone, Hertzian contact, Contact overloading,

1. Introduction

Surface or case hardening is commonly used to improve the wear resistance of mechanical parts or structural elements subjected to contact loading. Case hardening creates a non-uniform spatial distribution of hardness and consequently the yield strength of the material in the treated surface layers. Typically surface treatments, such as carbonitriding, carburizing, flame or induction hardening, etc. create a high hardness on surface and a decreasing hardness profile with depth. Elastic properties can usually be assumed constant. These materials are commonly called *plastically graded (PG) materials*.

Over the last few decades PG materials have attracted much attention in the research community in an attempt to characterize the treated surface by its effective response to indentation. During indentation a high contact pressure created by a sharp or spherical indenter forms a plastic zone directly under the

indenter and nonlinear dependence of the indentation depth on the contact load is typically the goal of numerical and experimental studies on PG materials (Suresh, 1997; Suresh et al., 1997; Giannakopoulos, 2002; Gu et al., 2003; Choi et al., 2008a; Choi et al., 2008b; Branch et al., 2011; Klecka et al., 2011; Moussa et al., 2012; Yuan et al., 2012; Klecka et al., 2013).

Although understanding the effective response of PG materials to indentation is extremely important from the tribological point of view, in practical applications an abnormal increase in the loads between hardened contacting parts can occur that does not necessarily lead to development of plastic zones on the contact surface, but nevertheless significantly affects the parts' durability.

Contacting mechanical parts are typically designed such that the stresses at any point of contact and adjacent areas do not exceed 50% - 90% of the elastic limit of the material (e.g. see Serensen et al., 1975; Roberts, 1978). This creates a situation where the values of the resultant non-uniformly distributed stresses acting in the near-contact zones are below the *local* elastic limit of the hardened material. In most cases, the elastic modulus of the material in the zones close to contact stays practically unchanged and the near- contact area can be considered as homogeneous elastic (although a variation in elastic modulus is also possible for some materials (e.g. Gu et al., 2003)). This ensures long-term operation of the strengthened parts without development of damage and failure. This situation is relevant under the condition that the parts work in a regular pre-designed regime.

However, the situation changes significantly when in some areas of the contact region the operating stress exceeds the *local* elastic limit and the material transfers into the elastic-plastic state. As an example, a very common issue in the steel industry is when the rolled sheet folds in the deformation zone between the rolls due to sheet breakage or non-uniform deformation of the sheet across its width, which can occur for several technological reasons. Practical research has established an unequivocal relationship between local overloading and subsequent damage in the case hardened rolls in the area of local overloads (Devyatchenko et al., 1982 ; Tsun, 1985). Analysis showed that the contact stresses increase three to five times when folds of strip with threefold or more thickness pass through the deformation zone, and the total forces increase even more rapidly (up to eight times) (Tsun, 1985). Nevertheless, these loading conditions are significantly milder than during the indentation tests mentioned above; case hardened rolls do not usually show any surface damage due to a single overloading, but demonstrate significant degradation in performance and high sensitivity to further loading resulting in premature, typically brittle, failures. High sensitivity of a roll's serviceability to a cyclic and even single overloading is directly related to the stress field redistribution in the elastic core of the PG material due to formation of plastic zones in the gradient transition zones.

According to the energetic strength theory (von Mises plasticity criterion), the transition of the material into a plastic state occurs when the intensity of shear stresses (effective stress) σ_i reaches the value of material yield strength σ_s. At the contact area between convex bodies, when the length of the contact is much smaller than the bodies' size, the distribution of σ_i as well as the distribution of the maximum shear stresses along the depth direction exhibits a maximum. In the simplest case, when there is no shear stress at the contact between the parallel cylinders and the diagram of normal contact pressure is symmetrical, the peak of the distribution is located on the axis of symmetry at depth $0.4 - 1.0$ of half the contact length, depending on the form of diagrams of contact pressure (0.785 in Hertz contact problem with elliptical distribution of contact pressure). The maximum value of the distribution is mainly determined by the maximum value of the contact stresses and the depth depends on the contact length. When tangential (for example, frictional) forces are operating at the contact the distribution maximum is shifted closer to the surface (Johnson, 1987).

Figure 1 schematically shows the distribution of the yield strength along the depth of hardened zone y (curve 1) and the values of σ_i on the symmetry axis of the loading area (curve 2), corresponding to regular work conditions.

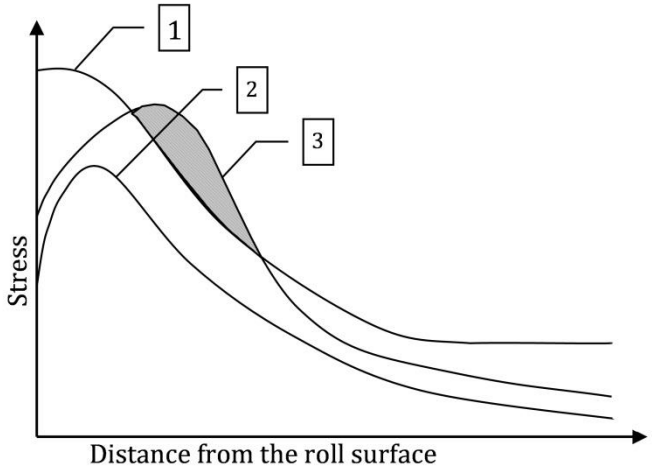

Figure 1. Location of the plastic zone along the depth of hardened layer of the roll. 1 - distribution of the yield stress of the material; 2 - distribution of effective stresses under normal rolling conditions; 3 - distribution of the effective stress in rolling of folds of the rolled strip.

Due to an overloading the contact stress and hence the effective stresses σ_i increase significantly (curve 3). In some depths σ_i becomes greater than the local yield stress (shaded area), which leads to a transition of the region to the plastic state. At this moment the original linear problem of loading the elastic homogeneous body turns into a nonlinear problem of deformation of a PG body, i.e. deformations

of an elastic body with a pliant elastic-plastic inclusion with moving boundaries influenced by the boundary conditions at the contact.

In this paper the problem of plastic zone formation in the gradient subsurface layers is addresses both experimentally and numerically. In Section 2 a systematic experimental program is described, that targets the hardness map and the corresponding yield stress map in the hardened surface layers in both the virgin and contact loaded disks, made of a case hardened chromium tool steel. The experimentally estimated distribution of the yield stress with depth is used in Section 3 for numerical FE analysis of a PG half-plane with a stress field perturbation due to formation of plastic zones in the gradient layer. The results are compared with stress fields in a homogeneous elastic body under the same loading conditions, typically assumed in design procedures. Discrepancies between the stress fields in the two schemes are observed and discussed.

2. Experimental observation

The experimental program was carried out on surface hardened discs 2 mm thick and 60 mm in diameter. The disks were cut from a chromium tool steel (2% of chromium and 0.9% carbon) cylinder, which was quench-hardened with high-frequency heating to a temperature of 880^{o}C, cooling in water, followed by tempering at 120°C temperature. The cylinder was sliced and the disks were ground and polished on both sides.

Micro-hardness (Vickers) test was next performed over the depth of 9 mm from the circumferential surface. The hardness variation with depth from the circumferential surface of the disk is shown in Figure 1 to indicate the measured depth of the quench-hardened zone of 3-3.5 mm (about 11% of the radius of the disks).

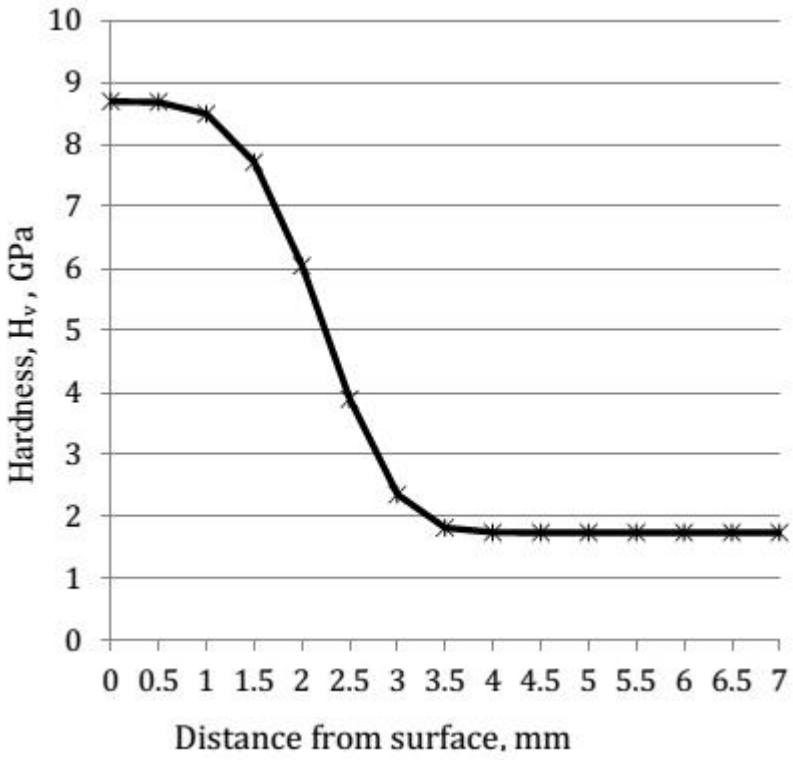

Figure 2. Distribution of hardness in the surface layer of the discs

The discs were loaded in a mechanical press according to the scheme shown in Figure 3. To create close to plane strain conditions the discs were clamped between two additional discs of the same diameter, but 10 times thicker than the studied discs. Two contact inserts having different hardness were used on the opposite sides of the discs in order to simultaneously obtain different contact conditions: hard alloy (WC– 6% Co) was used for the upper contact loading, while mild steel (0.08% carbon) was used for the bottom contact loading. Formation of the plastic zones and their boundaries were determined by measuring the change in the local hardness due to plastic deformation (Del, 1971; Branch et al., 2011).

In preliminary experiments, loading of the discs with line pressures of $2.0 - 3.0$ kN/mm (per unit thickness of the disk) did not change their hardness at any point. Loading of the disks with line pressure of $5.0 - 6.0$ kN/mm led to a noticeable change in the material hardness in the vicinity of the two contacts. Due to this load the top contact was subjected to an average contact pressure of $1.7 - 2$ KN/mm^2 leading to a contact length of 3 mm, while the bottom contact was subjected to an average contact pressure of $0.8 - 1$ KN/mm^2 leading to a contact length of 6 mm. These loading conditions were chosen for characterization of the plastic zones.

After loading one side of the disc was re-ground and polished to restore the clarity and flatness of the surface under inspection. Surface treatment was carried out with ample cooling to prevent heating and thermal influence on the hardness of hardened areas of the disk. Hardness test was performed on the

restored side in the contact area of 15 mm and a depth of 9 mm using micro-hardness tester (Vickers hardness test) with the indenter load of 1N and 0.5 mm spatial step. Increase in the local material hardness compared to the unloaded disks (Figure 1) was recorded.

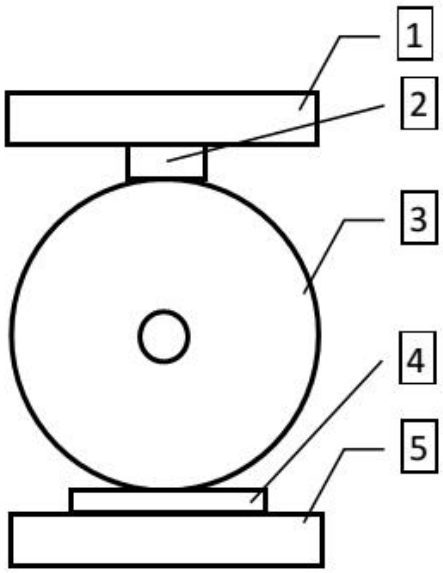

Figure 3. Disk loading scheme: 1&5 - press plates, 2 – hard alloy insert, 3 – disc, 4 - mild steel insert.

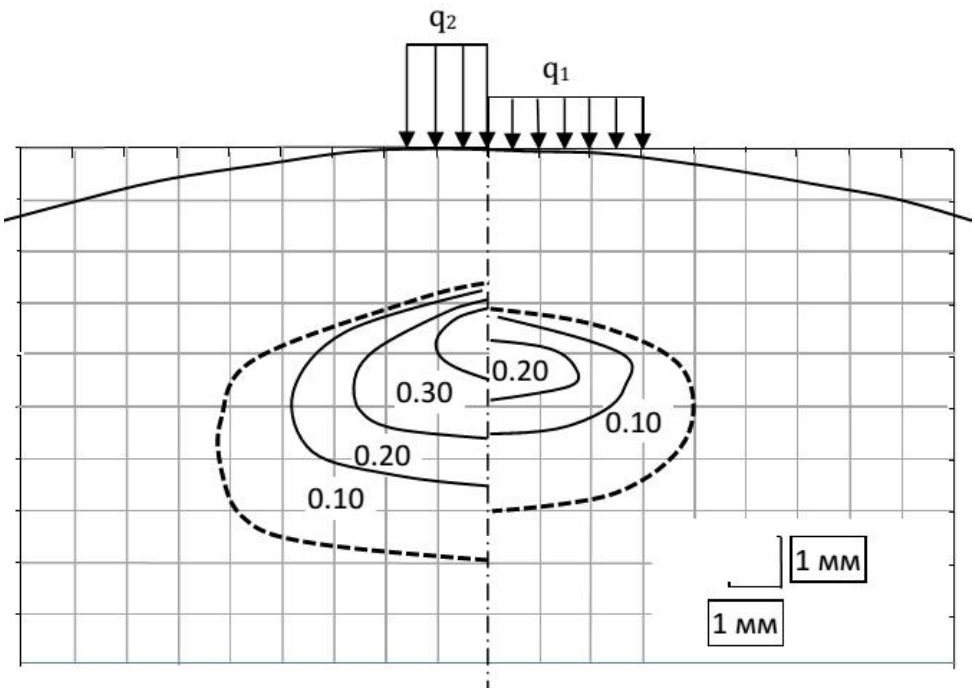

Figure 4. Plastic deformation zone in the loaded disc. The numbers on the contour lines indicate increase in the hardness of the material δHv (GPa) as a result of plastic deformation.

Figure 4 shows the distribution of the hardness increment in the subsurface layers of the disks after the loading. The areas of plastic deformation at the average load $q_1 = 0.8\ \mathrm{KN/mm^2}$ with the contact length of 6 mm, and at the average load $q_2 = 1.6\ \mathrm{KN/mm^2}$ with the contact length of 3 mm are shown on the right and on the left side from the symmetry axis, respectively. Boundaries of the plastic zone shown by the dashed thicker line are drawn through the points at which the local hardness was the same as for the virgin material. The location of the contour lines was determined by interpolation of the hardness increment values at the grid points using the method of least squares. The confidential interval of the contour line locations is $\delta = \pm 0.1$ mm with reliability of 0.9.

As can be seen from the data, plastic zones of oval form were formed in the surface layers of the disk. Maximum increase in local hardness, and hence the maximum plastic deformation were developed at depths *considerably greater* than the depth of the maximum values of the effective stress predicted by the elastic contact problem solution. Namely, according to the Hertz solution maximum effective stress and consequently strain are reached at the depth of 0.785 of half contact length b (e.g. see Williams et al., 1999), but in the experiments maximum hardness increment and hence maximum strain were observed at the depth of (1.5 - 2) b. This is apparently due to the descending nature of the distribution of material hardness in the transition zone of the hardened layer.

Since the hardness change in the region of plastic deformation of hardened steel can be caused by either plastic deformation or microstructural transformations (decomposition of retained austenite), X-ray diffraction analysis of structures of the near-contact and adjacent areas was also carried out for the studied specimen in both the original and loaded states according to the scheme shown in Figure 3. Residual austenite was not detected in the models. Therefore, all the increase of hardness was solely caused by plastic deformation.

The same thin discs were used in alternative experimental settings to observe formation of plastic zones under conditions close to plane stress. Loading of the disks was implemented without the lateral clamping discs. The loaded disk was instead supported along of the horizontal large diameter on its both sides (Figure 5) in order to ensure the longitudinal stability of the disk. The distance from the side pivots to the formed plastic zones was at least three times the sizes of the plastic zone, which provided the conditions close to plane stress. Parameters of disk loading and hardness measuring were the same as for plane strain conditions.

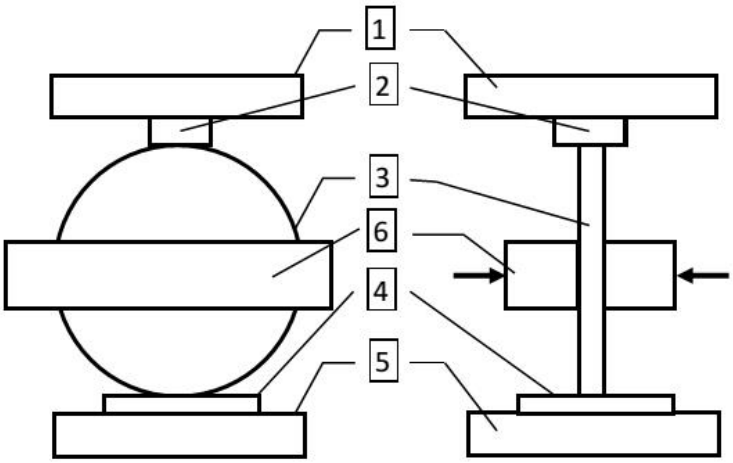

Figure 5. Schematic diagram of discs loaded under plane stress conditions:1,5 - press plates, 2 – hard alloy insert, 3 - disc 4 - mild steel insert; 6 - side supports of the disc for lateral stability. Arrows show that the side supports are compressed.

Figure 6 shows the distribution of hardness increments in the surface layers of the disks after loading with the average load $q_2 = 1.6$ KN/mm^2 for the contact length of 3 mm. The area of plastic deformation under the plane strain conditions is shown on the left of the symmetry axis, and the one under plane stress conditions is shown on the right. The boundary of the plastic zone, drawn through the points of zero hardness increment, is shown by a thicker dashed line.

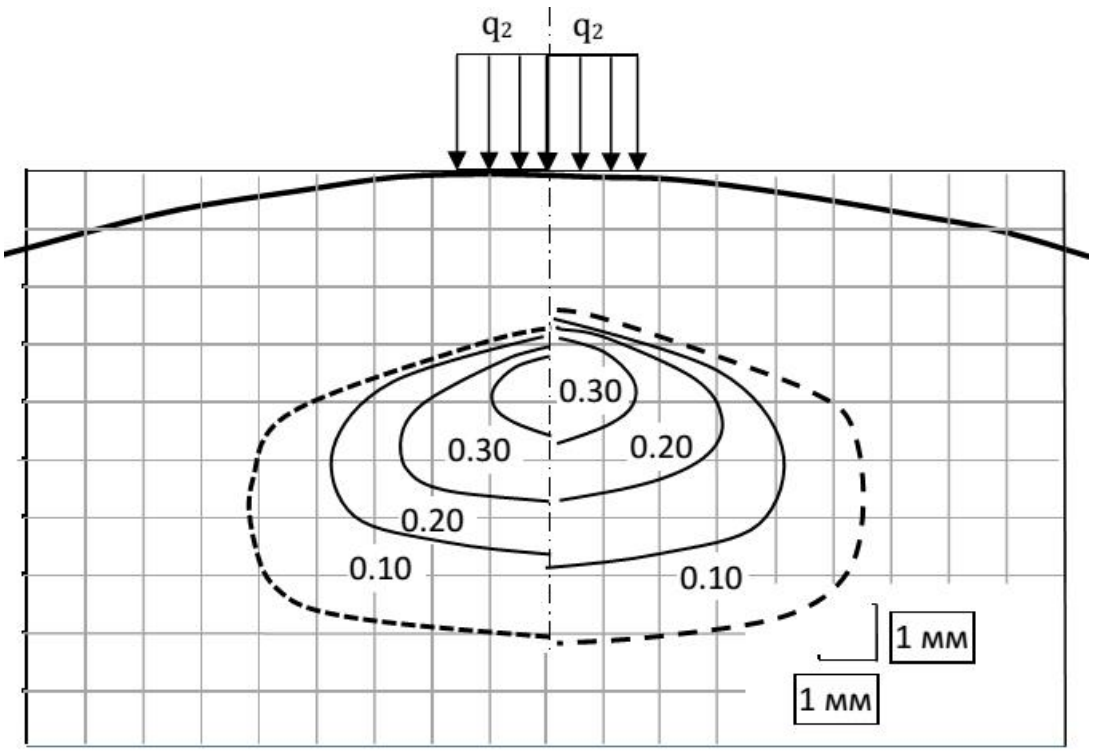

Figure 6. Plastic deformation zone in the disk loaded in plane strain (left) and plane stress (right). The numbers on the contour lines indicate increase in hardness of the material δH_v (GPa) as a result of plastic deformation.

As it can be seen from the data, the shape and size of the plastic zones, as well as the characteristics of the hardness increments distribution due to the plastic deformation under the plane strain and plane stress are very similar, which is in line with the elasticity problem were the solutions are different by a factor depending solely on the value of Poisson's ratio (e.g. see Johnson, 1987). Small differences in the distributions can also be explained by the counter influence of factors such as the unconstrained lateral displacement under plane stress and material hardening with increasing strain.

In order to determine the values of residual effective plastic strain ε_i^p formed by the local radial loading of surface hardened discs, calibration curves of hardness increase of chromium steel with different initial hardness as a function of plastic strain were built. Experiment specimens, cylinders with 10 mm diameter and 30 mm thickness, with an initial hardness in the range of 1.8 - 4.0 GPa were loaded until their residual plastic strain reached $\varepsilon_h^p = 0.2\% - 4.0\%$. In the case of simple uniaxial compression $\varepsilon_i^p = \varepsilon_h^p$ (Thomsen et al., 1965). To ensure the simple uniaxial compression mode the specimen ends were lubricated with palm oil supplemented with 10% molybdenum disulfide. On two diametrically opposite sides of the samples 4 mm wide parallel faces were created for hardness measurements. Each hardness value was determined as the arithmetic mean of 8 - 14 measurements, which allowed us to obtain the mean square error of the result of ± 0.013 GPa. The resultant calibration curves are shown in Figure 7.

Based on the experimentally found relationship between the residual plastic strain ε_{ip} and increase in hardness in the cylindrical samples, the contour lines of hardness increments in loaded discs (Figure 4) were converted to corresponding contour lines of the effective plastic strain ε_{ip}. This was used for confirmation of validity and comparison of the results of the finite element model, described in the next Section, as can be seen in Figure 11.

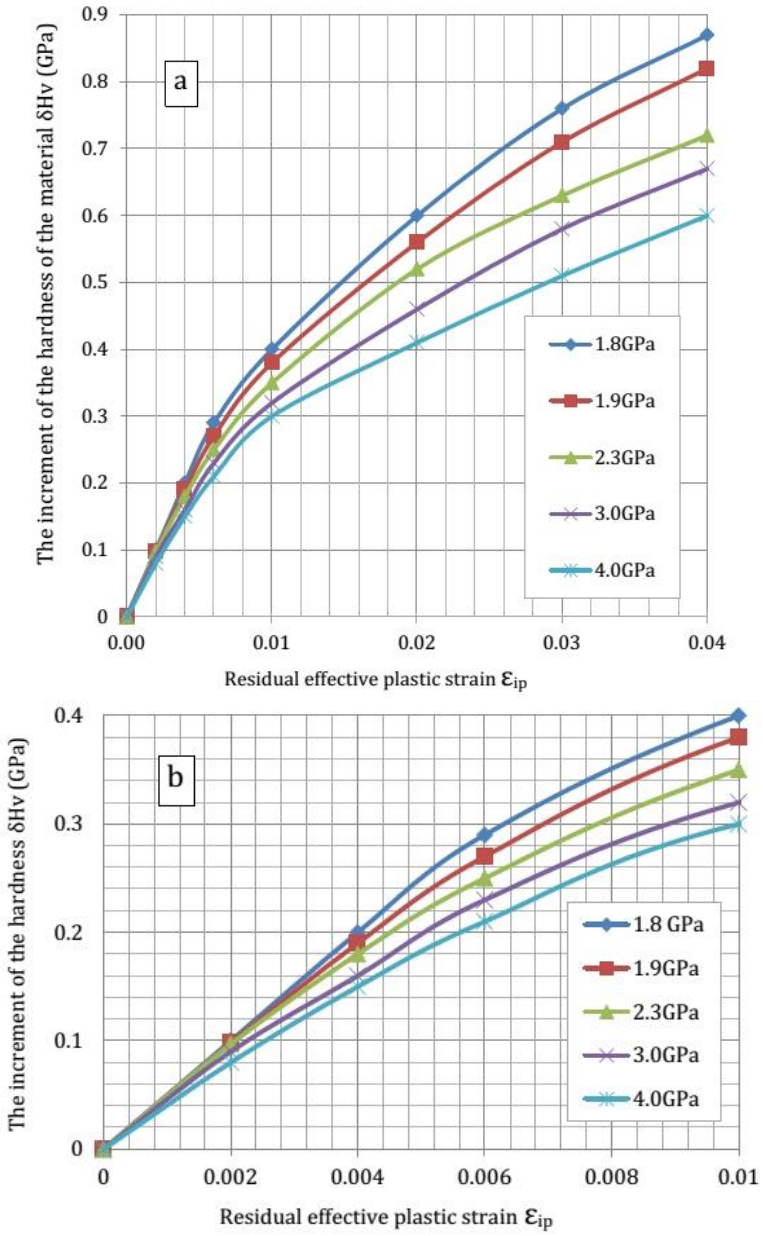

Figure 7. Hardness increase δHv of Chromium steel with various initial hardness ($\mathbf{1.8-4.0}$ GPa) vs. residual effective plastic strain $\boldsymbol{\varepsilon_i^p}$: (a) $\boldsymbol{\varepsilon_i^p = 0\text{–}0.04}$; (b) zoom on $\boldsymbol{\varepsilon_i^p = 0\text{–}0.01}$

3. Finite element analysis

Numerical modeling of the contact problem of deformation of a PG material was carried out by finite element method using commercial software 'Comsol-4' (Zimmerman, 2004; Baker, 2012; Pryor, 2012). The fact that there are no fundamental differences in the contact problems in plane strain and plane stress allows us to use a two-dimensional plane stress model for numerical analysis of deformation of PG solids. This greatly simplifies and accelerates numerical simulations, without loss of generality of the results.

The problem of local contact loading of a PG half-plane (i.e. in plane stress) is considered, when an elastic circular disk of a certain diameter was pressed onto the half-plane, forming a contact zone of length $2b$ along the straight upper boundary. The straight boundary eliminates the influence of the contact surface curvature of the PG body on the distribution of stress/strain fields in the near-contact zones. The contact was treated as frictionless. The influence of contact friction, the shape of the distribution of contact stresses along the contact and the curvature of the contact surface will be discussed elsewhere.

The origin of coordinate system is placed in the middle of the contact area, the *X* axis points horizontally to the right along the contact surface and the axis *Y* upwards being the axis of symmetry.

In the present simulations the length of contact zone $2b$ was chosen to reproduce the contact settings of the experiments described in the previous Section, while the corresponding required radius R of the pressing disk was determined from the Hertz solution

$$b = \sqrt{\frac{8F_n R}{\pi E_e}}, \tag{1}$$

where F_n is the force pushing the disk onto the half-plane (total contact force per unit thickness) and E_e is the combined Young's modulus, determined by the expression

$$E_e = \frac{2E_c E_p}{(E_c + E_p)(1-\nu^2)}. \tag{2}$$

Here E_c is the Young's modulus of the disk material, for steel E_c =210GPa; E_p is the modulus of the half-plane material, for steel E_p =210GPa; ν is the Poisson's ratio, for steel $\nu = 0.3$. The contact length was assumed to be the same as in the experiments on the surface loaded hardened discs, i.e. $2b$ = 3 mm; 6 mm for further comparison of the numerical and experimental results. The forces on the disk where chosen as F_n =3 kN, 6 kN and 10 kN. For the force of $F_n = 6$ kN and $2b = 3$ mm the radius of the disk under pressure is R =33.8 mm, and for $2b$=6mm the radius of the disk is R=135.5mm.

The elliptic Hertzian pressure distribution along the contact is given as

$$p_i = p_{max}\sqrt{1-\left(\frac{x}{b}\right)^2}, \tag{3}$$

where p_{max} is the maximum pressure at $x = 0$, determined by the expression

$$p_{max} = \sqrt{\frac{F_n E_e}{2\pi R}} \tag{4}$$

The yield strength distribution $\sigma_{sy}(y)$ with the depth from the surface of the half-plane (along the Y axis) was assumed to be most accurately described by the following Weibull-type exponential function:

$$\sigma_{sy} = \sigma_{s0}\left(0.2 + 0.8e^{ay^n}\right), \tag{5}$$

where the parameters are chosen to reproduce the distribution obtained from the hardness measurements on the unloaded surface hardened disks. These parameters were estimated on the basis of the distribution of the microhardness of the surface layer material of the samples (Figure 2) described in the previous Section. The value of the yield stress of the material related to the value of its hardness is estimated by the method Brinell HB (Del, 1971)

$$\sigma_s = 0.32\ HB$$

The hardness HB is determined using empirical harness conversion charts between the hardness on the Vickers scale and Brinell (Oberg et al., 1979) along with the fact that the value of Vickers hardness (under a load of $100 - 200$ N the with the diamond pyramid indenter) is $15 - 25\%$ lower than the microhardness values determined under a load of $1 - 2$ N with an identical pyramid (Del, 1971). In Equation (5) σ_{s0} denotes the maximum value of yield strength at $y = 0$. For heat-treated hardened chromium steel with a hardness of about $8.5 - 9$ GPa the accepted value of the offset yield strength is $\sigma_{s0} = \sigma_{0.2} = 1.8$ GPa. Other factors in (5): a – is the scale parameter, $a = -0.04$; n – is the shape parameter, $n = 3$.

Behavior of the material beyond the elastic limit is approximated by adopting linear strain hardening. The average value of the hardening modulus at strains of $0 - 10\%$ is accepted at $m = 3 \times 10^9$ GPa, based on the graph for micro-hardness increments of the samples due to plastic deformation (Figure 7)..

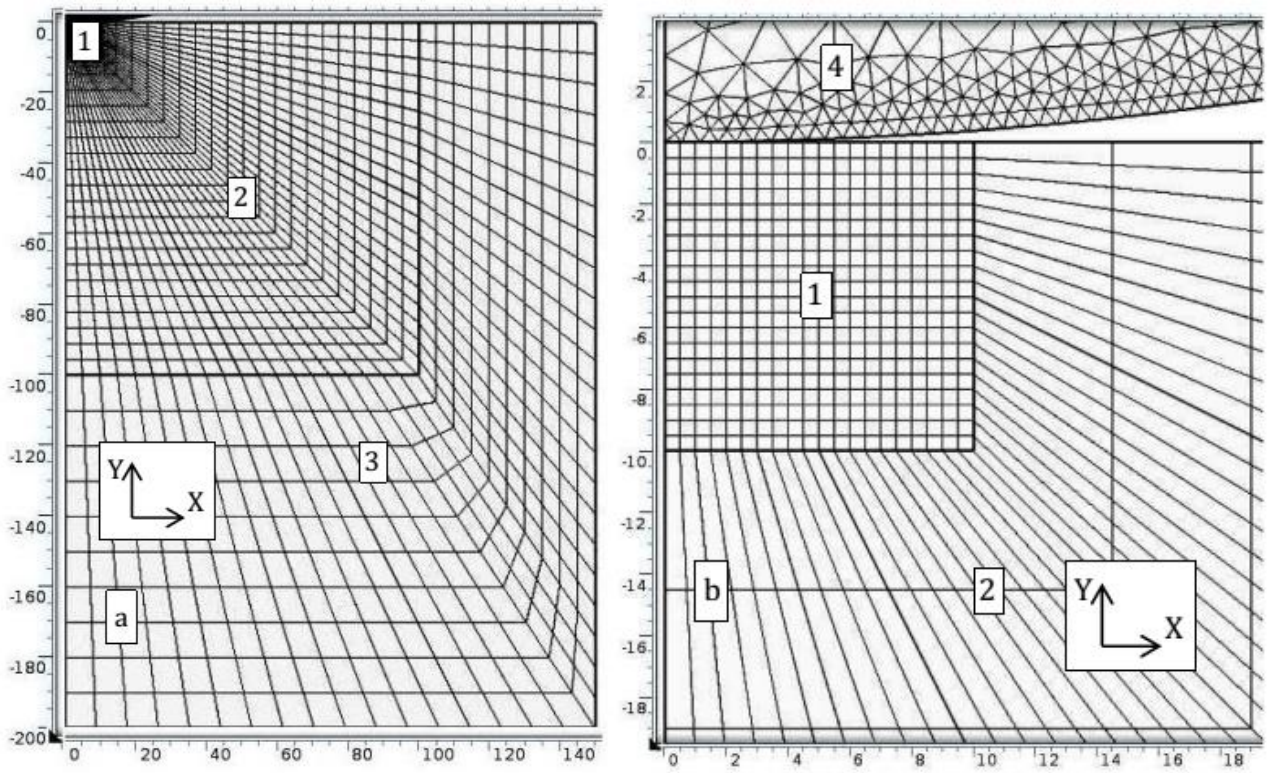

Figure 8. Finite element mesh for the solution of the contact problem. (a) - general view of the mesh; (b) - enlarged view of the contact region of the grid.

In order to see the effect of the subsurface plastic zones on the near-contact stress field, the solution of the contact problem for a PG half-plane is compared to the solution of the contact problem for a half-plane in which the yield strength of the material are assumed constant at 1.8 GPa, same as the value at the surface of the PG half-plane. The loading disk is assumed to be perfectly elastic.

Due to the symmetry of the model about the vertical axis the calculations were performed for the right half of the model. The size of the truncated domain of the modelled half-plane was chosen under the following considerations. For the solution of the elastic contact problem of a loaded half-plane of infinite size the zone with significant values of strains and stresses (more than 10% of their maximum values) for the contact length of 3 mm and 6 mm lays inside the rectangle ($x = 15$ mm, $y = -20$ mm), when the values of the strain and stress of more than 50% of the maximum values of these parameters are obtained in the contact zone with the dimensions of ($x = 7$ mm, $y = -9$ mm). In order to minimize the influence of the size of a half-plane on the results the size of the modeled half-plane was chosen 10 times larger than the rectangle with significant values, i.e. ($x = 150$ mm, $y = -200$ mm). The half-plane FE model was constructed in the form of a grid with variable mesh size and was divided into 3 regions (Figure 8). The size of contact region area, where the expected value of the strain and stress were more than 50% of the maximum values of these parameters with maximum gradients of change, was chosen as 10x10 mm (zone 1 in Figure 8) and was meshed with a grid of square elements of length 0.5 mm, i.e. each side of the square was divided into 20 elements. The intermediate region 2 with the increased

length of the elements was located between the coordinates ($x = [10{,}100]$ mm, $y = [-10, -100]$ mm). Each side of the obtained polygon was divided into 20 elements, and the grid is formed as shown in Figure 8. The peripheral region 3 ($x = [100, 150]$ mm, $y = [-100, -200]$ mm) is approximated by a grid with large step, as shown in Figure 8. Zone 4 is the loading disk with a mesh of triangular elements.

In all the analyzed cases the diagrams of the contact stresses distribution along the contact zone, determined analytically by equation (3) and from the FE model, had similar values for both homogeneous and PG half-planes. Examples of diagrams of contact stress distribution along half the length of the loading area are shown in Figure 9. As expected, contact pressure was reduced almost twice when the length of the contact surface was increased from 3 to 6 mm.

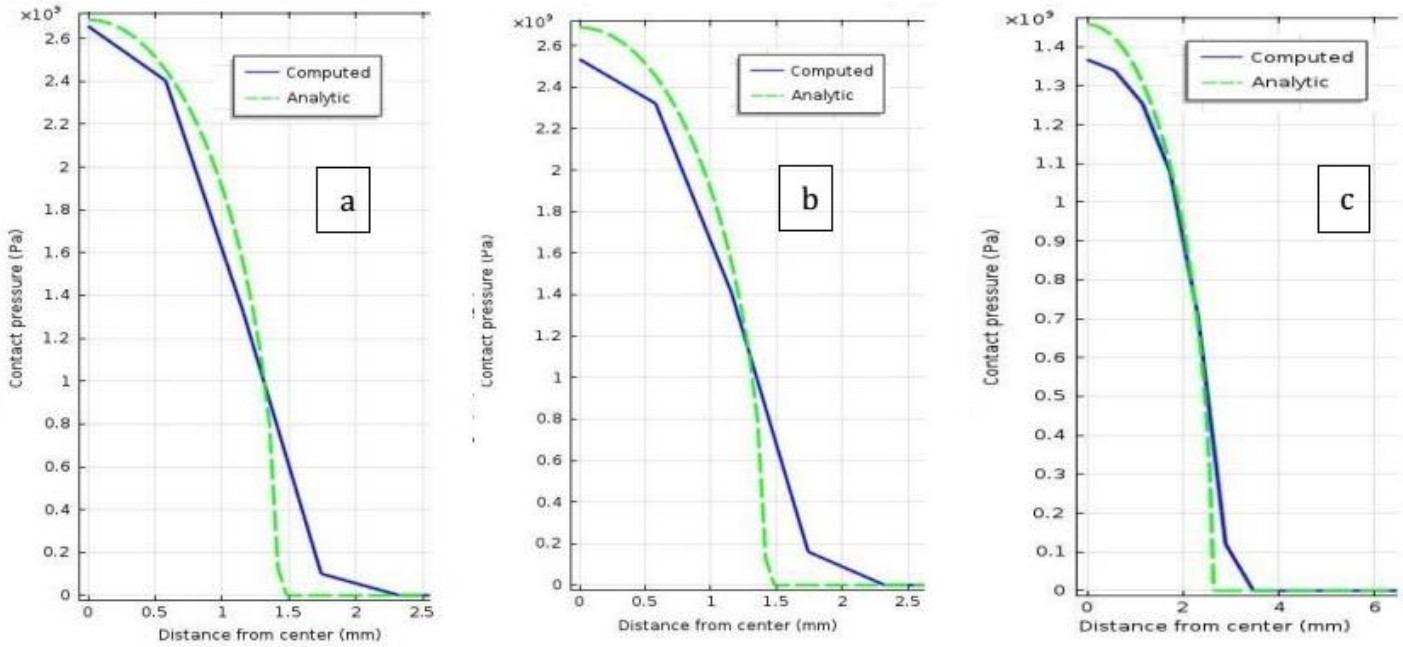

Figure 9. Diagrams of contact stress distribution along half the length of the loading area: (a) homogeneous elastic half-plane with high constant yield strength of the material $\boldsymbol{\sigma_{s0} = 1.8}$ GPa, loading force $\boldsymbol{F_n = 6}$ KN, the length of the contact area $\boldsymbol{2b = 3}$ mm; (b) anisotropic half-plane with a variable yield strength of the material $\boldsymbol{\sigma_{sy}}$, loading force $\boldsymbol{F_n = 6}$ KN, length of the contact area $\boldsymbol{2b = 3}$ mm; (c) PG half-plane with a variable yield strength of material $\boldsymbol{\sigma_{sy}}$, loading force $\boldsymbol{F_n = 6}$ KN, length of the contact area $\boldsymbol{2b = 6}$ mm.

Figure 10 shows the distribution of the effective stress σ_i in the homogeneous elastic half-plane along the symmetry axis Y at different contact lengths $2b$ and loading forces F_n. It also shows the curve of the yield stress of the material σ_{sy} along the Y axis in the PG half-plane. Figure 10 indicates that under load of $F_n = 3$ KN the values of effective stress σ_i does not exceed the yield strength of the material σ_{sy} in the PG half-plane at any point. At a higher loading efforts F_n there are areas where the value of the effective stress σ_i exceeds the yield strength of the material σ_{sy} at a certain depth. In these areas the material enters into the plastic state.

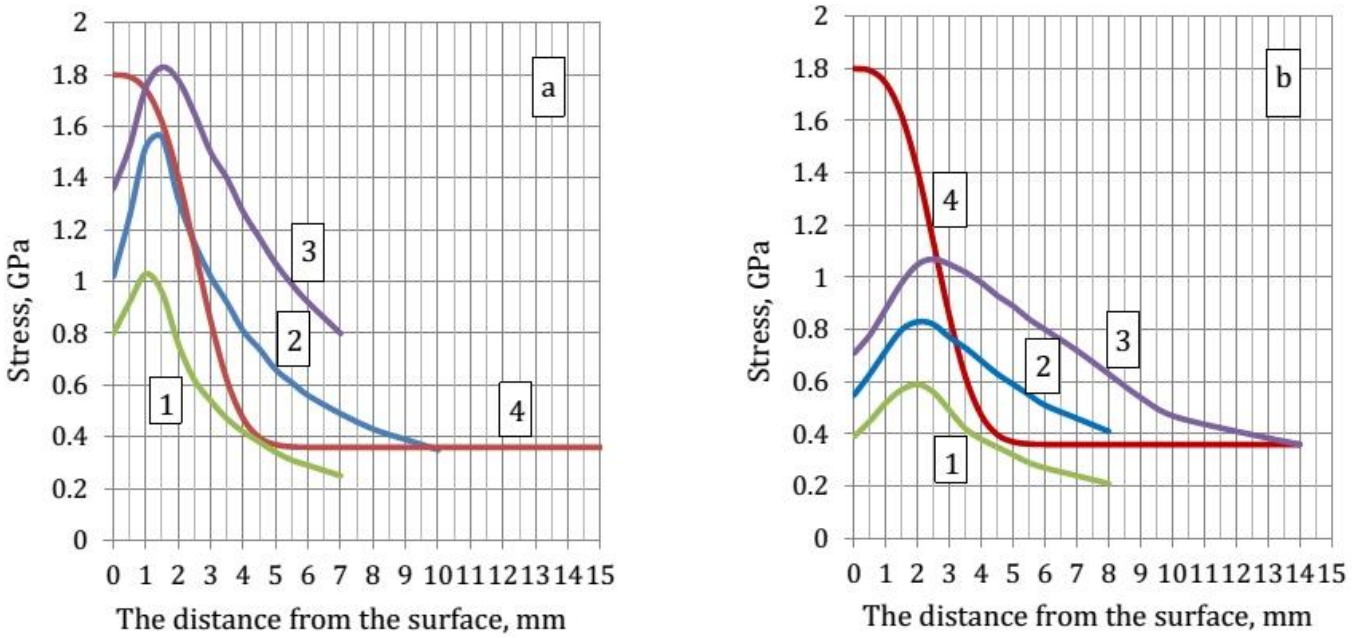

Figure 10. Distribution of effective stress $\boldsymbol{\sigma_i}$ (in an isotropic elastic half-plane), and the yield strength of the material $\boldsymbol{\sigma_{sy}}$ (in the homogeneous half-plane) with depth of the contact zone along the axis of symmetry Y. (a) contact length $\boldsymbol{2b = 3}$ mm; (b) contact length $\boldsymbol{2b = 6}$ mm; 1 - load $\boldsymbol{F_n = 3}$ KN; 2 - load $\boldsymbol{F_n = 6}$ KN; 3 - load $\boldsymbol{F_n = 10}$ KN; 4 - distribution of the yield stress of the material $\boldsymbol{\sigma_{sy}}$ in the PG half-plane.

Occurrence, the shape and size of the plastic zone were determined by non-zero values of the second invariant of plastic strain tensor, which characterizes the effective plastic strain ε_i^p. Plastic strains ε_{ij}^p were determined as the difference between total strains ε_{ij} and elastic strains ε_{ij}^e. Formation of a plastic zone during loading of the PG half-plane is detected for the contact lengths of $2b = 3$ mm and 6 mm and loading forces of $F_n = 6$ KN and 10 KN (for example, see Figure 11). For comparison, Figure 11 shows the distribution of the calculated effective plastic strain ε_i^p determined by finite element analysis with superimposed contour lines of the effective plastic strain ε_i^p estimated from the experimental data. It should be noted that the shape, size and location of plastic zones observed in the experiments and FE simulations are in satisfactory agreement (Figure 11).

Due to the spatial variation of the plastic properties plastic zones are displaced deeper relative to the maximum of the effective stress σ_i towards the layers with lower yield strength, and above them a sufficiently extended narrow near-surface region remains in the elastic state. This area works essentially like a beam on a compliant foundation. Therefore, when a plastic zone emerges the stress-strain state of the PG half-plane changes significantly. In the contact area in the distribution of effective stress σ_i there are two maxima, equidistant from the axis of symmetry Y (Figure 12). The distance between the maxima increases with increasing length of the contact surface and the loading force.

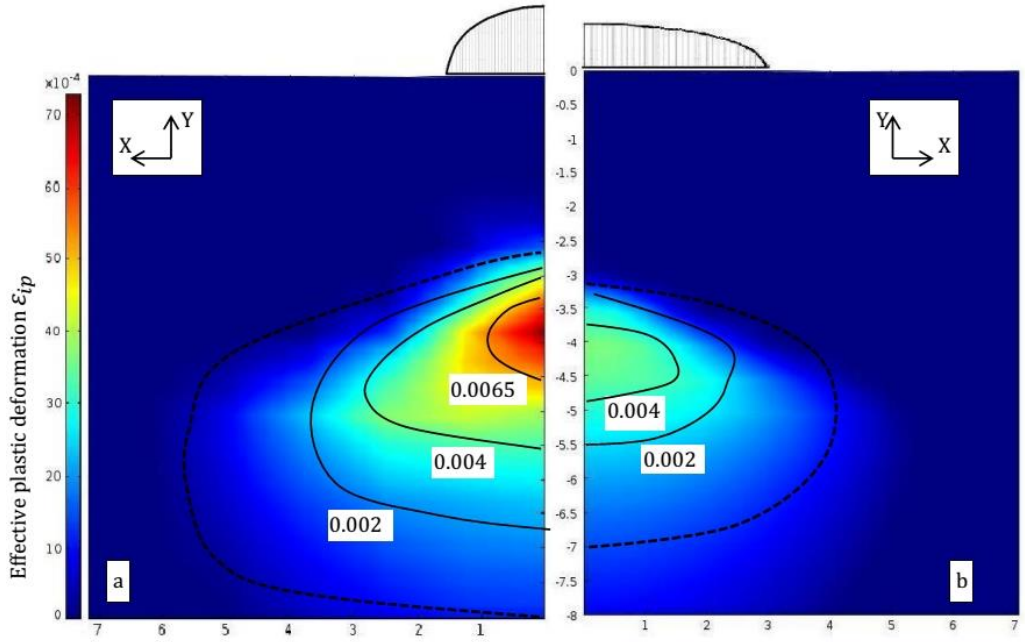

Figure 11. Plastic zone in the PG half-plane for the loading force $\boldsymbol{F_n = 6}$ KN and: (a) contact area length $\boldsymbol{2b = 3}$ mm and (b) **6** mm. Color map represents the level of effective plastic strain, dark blue field - zone of zero plastic strain. *X* an *Y* coordinates are in mm.

Due to the loading force $F_n = 3$ KN the distribution of effective stress σ_i in the PG half-plane coincides exactly with the distribution of the effective stress in the homogeneous elastic half-plane under identical loading conditions (cf. Figure 10 and Figure 13) due to the fact that in both the cases the effective stress does not exceed the local material yield strength at any point. The distribution of effective stress σ_i has one maximum located on the Y axis.

At higher loads the elastic near-surface region in the vicinity of the Y axis undergo some unloading and the distribution of σ_i forms two peaks (Figure 13). Interestingly, close to the origin of the coordinate system stress intensity substantially increases as compared to the homogeneous elastic half-plane, and becomes more intense with the increasing loading force (cf. Figure 10 and Figure 13).

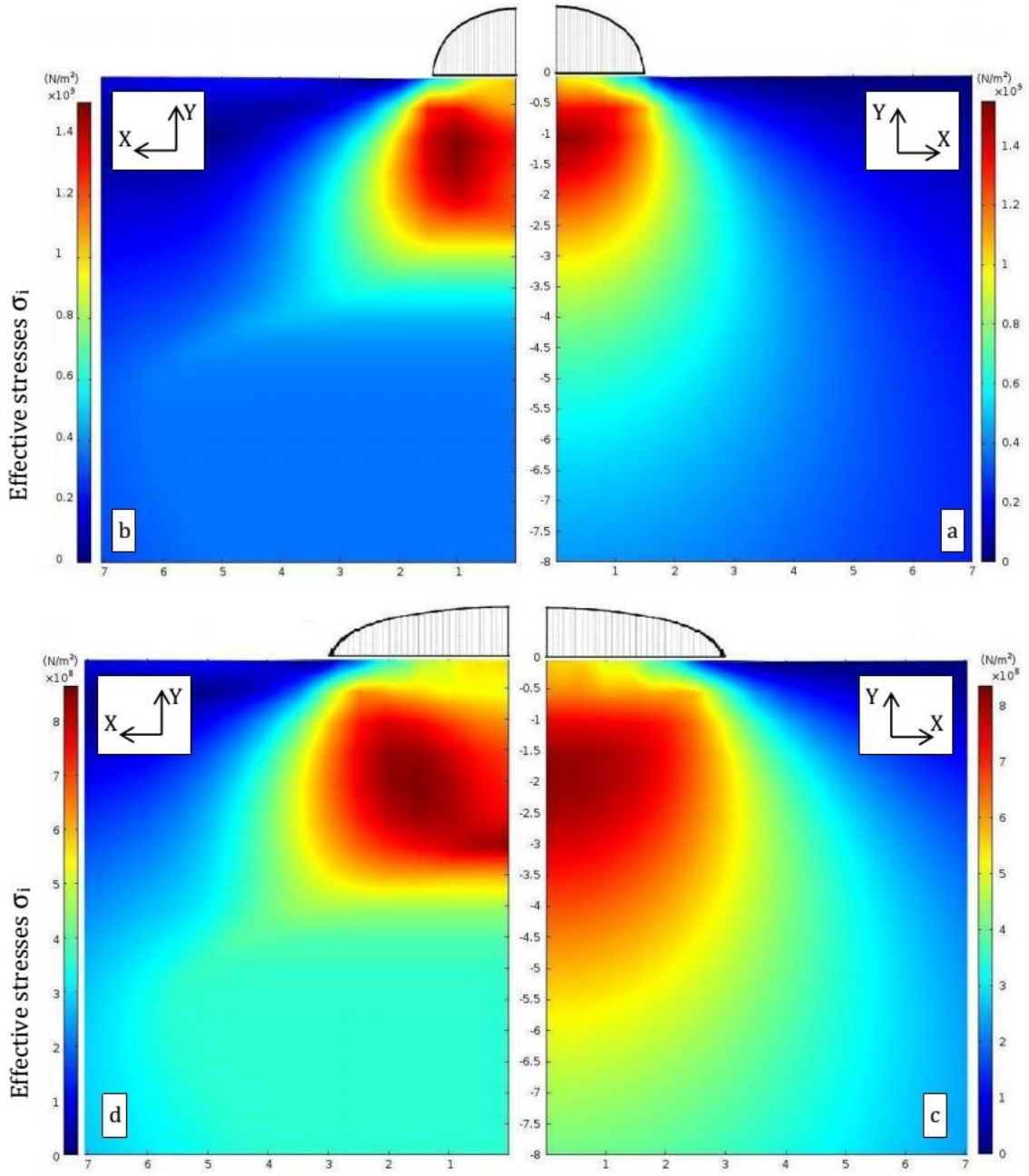

Figure 12. Distribution of effective stress $\boldsymbol{\sigma_i}$ in (a, c) homogeneous elastic half-plane and (b, d) PG half-plane for the contact length of (a, b) $\boldsymbol{2b = 3}$ mm and (c, d) $\boldsymbol{6}$ mm. The loading force $\boldsymbol{F_n = 6}$ KN. X and Y coordinates are in mm.

The near-surface region in the contact area, remaining elastic, is in a highly loaded state, particularly with a short-length contact and high contact loads (Figure 13a). The mostly stressed zone of this area is its lower boundary (or the upper boundary of the plastic zone). Here the hardened material is in the elastic state and under the influence of stresses, the cumulative effect of which leads to the effective stress σ_i close to the yield strength. Hardened steel, which has low plastic capacity, is very sensitive to the action of tensile stresses that might lead to cracking and fracture. The maximum tensile stress σ_x acts exactly at the depth of the upper boundary between the elastic and plastic zones (Figure 14a). Tensile

stresses σ_x develop also at the free surface in the vicinity of the contact loading area (Figure 14b). Figure 15 shows the maximum values of tensile stress σ_x at the upper boundary between the elastic and plastic zones (a) and on the free surface in the vicinity of the contact loading area (b) under different loading conditions. As can be seen from the presented data, the maximum values of tensile stress σ_x mostly depend on the load force F_n for small length of contact and high contact stresses only when a closed-shape plastic zone forms beyond the surface.

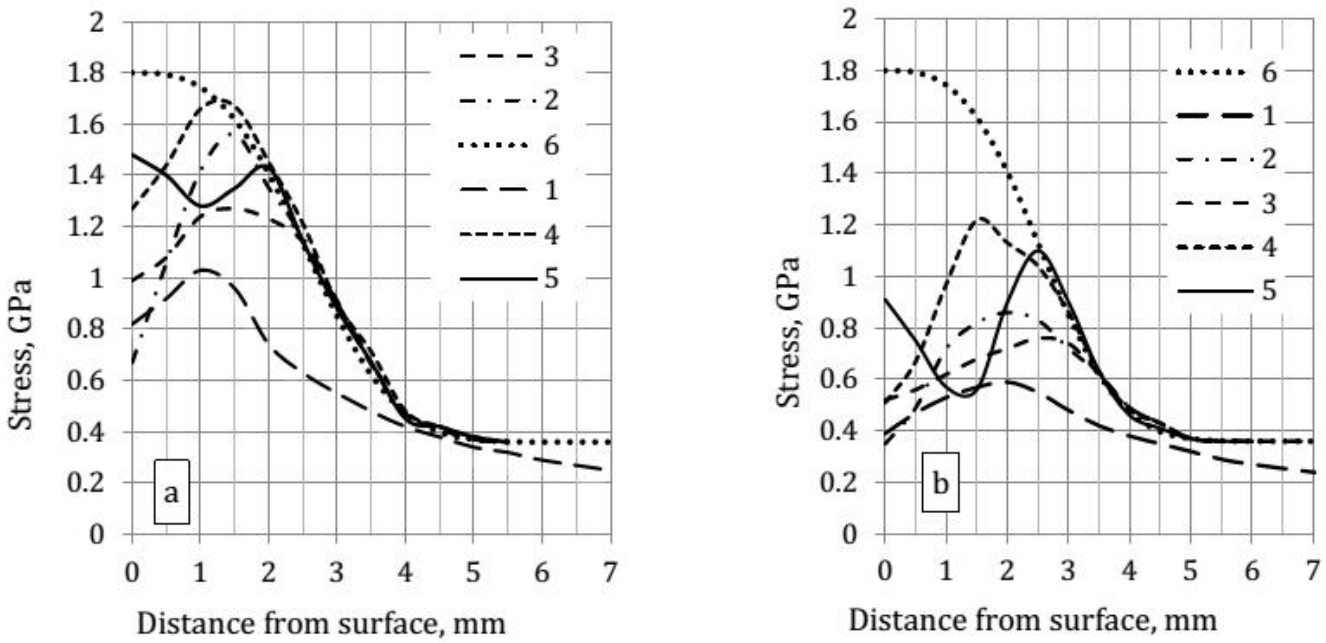

Figure 13. Distribution of effective stress $\boldsymbol{\sigma_i}$ in the PG half-plane with depth for the contact length (a) $\boldsymbol{2b = 3}$ mm and (b) 6 mm:

1 – $\boldsymbol{\sigma_i}$ with depth for a loading force $\boldsymbol{F_n = 3}$ KN,

2 – $\boldsymbol{\sigma_i}$ with depth for a loading force $\boldsymbol{F_n = 6}$ KN along the line (a) $\boldsymbol{x = 1.3}$ mm and (b) $\boldsymbol{2.4}$ mm, passing through the peak of the distribution,

3 – $\boldsymbol{\sigma_i}$ for $\boldsymbol{F_n = 6}$ KN along axis $\boldsymbol{Y}$ ($\boldsymbol{x = 0}$ mm),

4 – $\boldsymbol{\sigma_i}$ for $\boldsymbol{F_n = 10}$ KN along the line (a) $\boldsymbol{x = 2.5}$ mm and (b) $\boldsymbol{x = 3.7}$ mm, passing through the peak of the distribution,

5 – $\boldsymbol{\sigma_i}$ for $\boldsymbol{F_n = 10}$ KN along axis Y (x = 0 mm),

6 – distribution of the yield stress of the material $\boldsymbol{\sigma_{sy}}$.

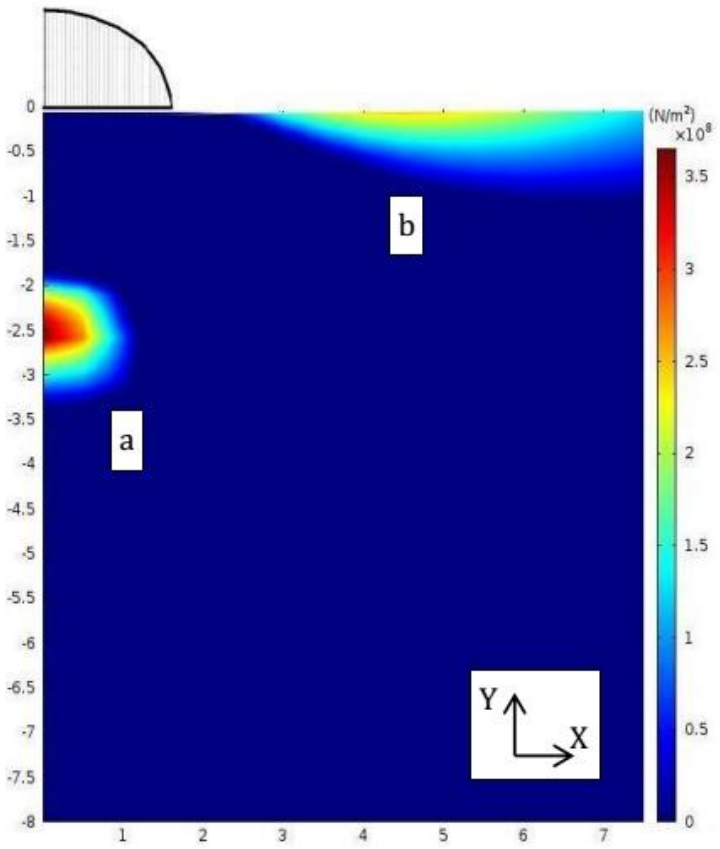

Figure 14. Zones of tensile stress $\boldsymbol{\sigma_x}$ (a) at the depth of the upper boundary between the elastic and plastic zones and (b) at the free surface in the vicinity of the loading contact area. Compressive stresses are not shown. Colour map represent the level of stress $\boldsymbol{\sigma_x}$, dark blue field - zone of zero and negative stresses. X and Y coordinates are in mm.

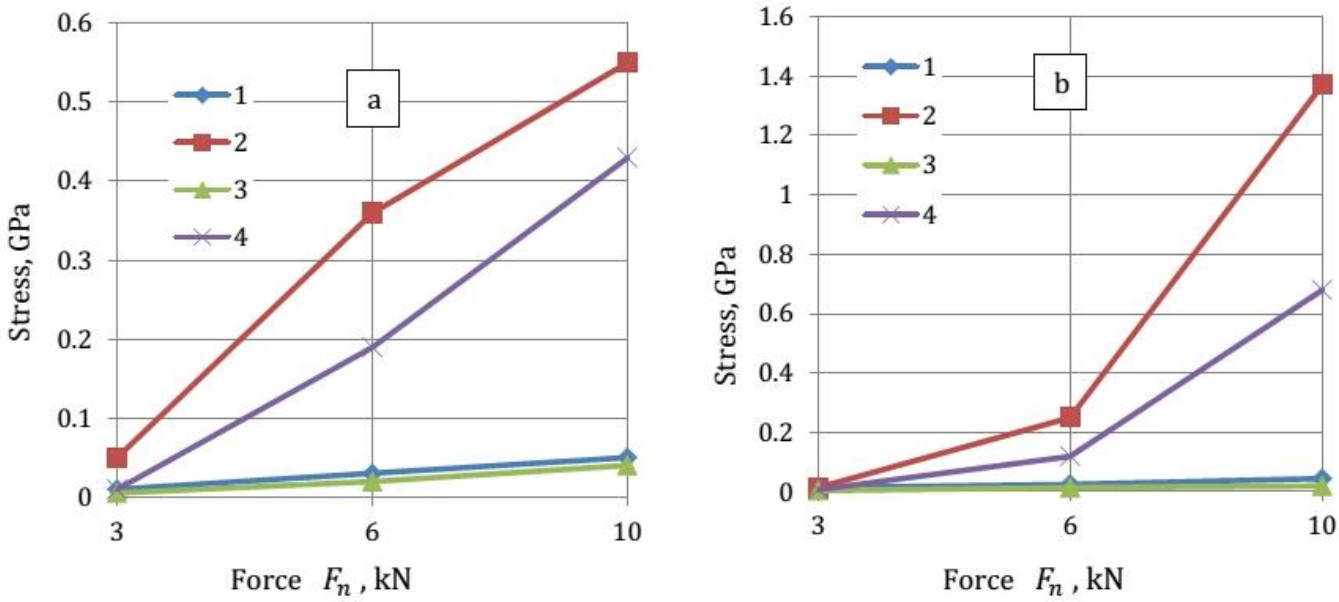

Figure 15. Maximum tensile stress $\boldsymbol{\sigma_x}$ (a) at the upper boundary between the elastic and plastic zones and (b) at the free surface in the vicinity of the of contact area for the various loading conditions: 1 - the length of the loading area $\boldsymbol{2b = 3}$ mm, homogeneous half-plane with a constant yield strength of $\boldsymbol{\sigma_{s0} = 1.8}$ GPa; 2 - the length of the loading area $\boldsymbol{2b = 3}$ mm, PG half-plane; 3 - the length of the loading area $\boldsymbol{2b = 6}$ mm homogeneous half-plane with a constant yield strength of $\boldsymbol{\sigma_{s0} = 1.8}$ GPa; 4 - the length of the loading area $\boldsymbol{2b = 6}$ mm, PG half-plane.

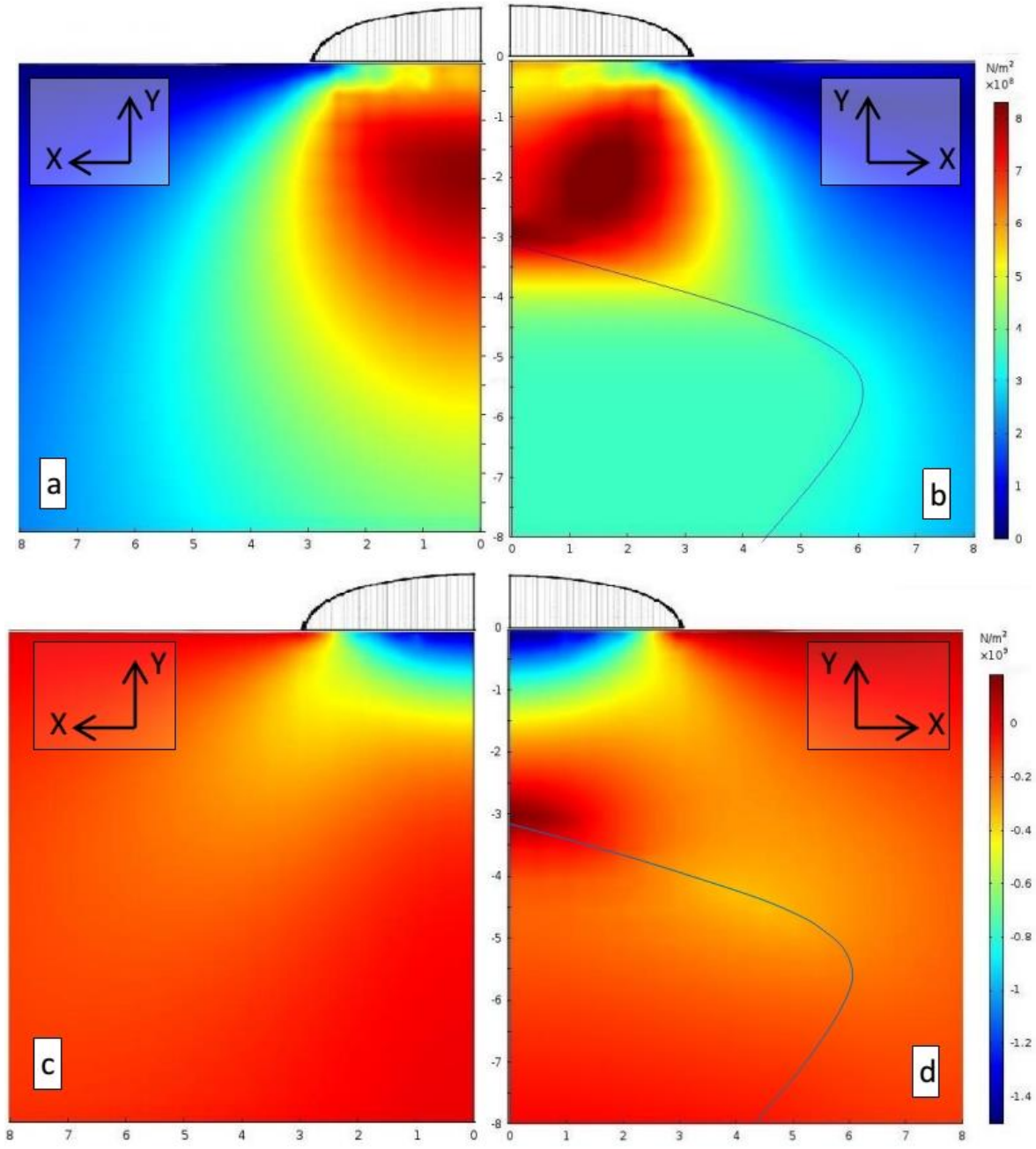
a
b
c
d
X
Y
N/m²
×10⁸
×10⁹

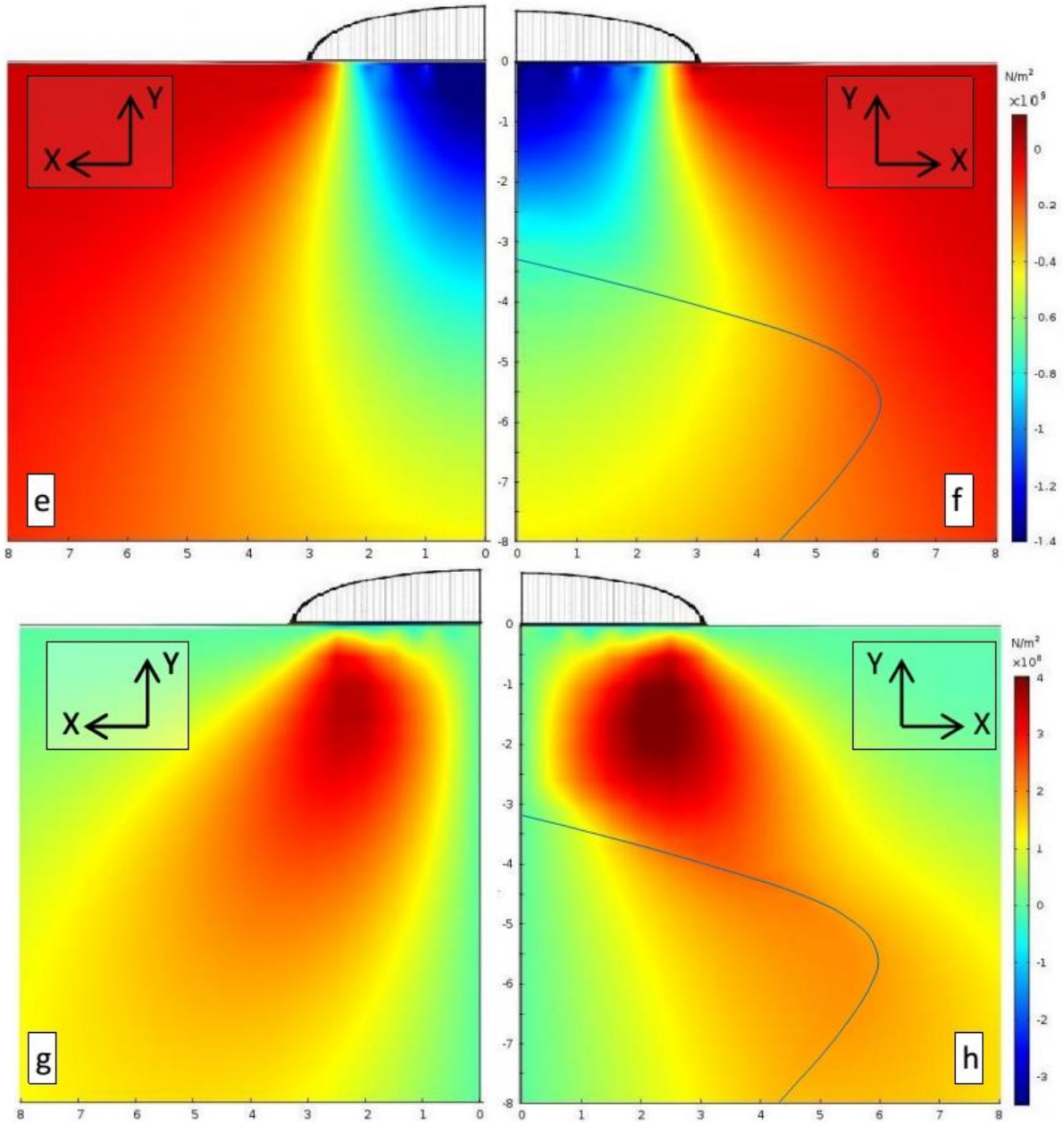

Figure 16. Distribution of effective stress $\boldsymbol{\sigma_i}$ (a, b) and the stress tensor components $\boldsymbol{\sigma_x}$ (c, d) , $\boldsymbol{\sigma_y}$(e, f) and $\boldsymbol{\sigma_{xy}}$ (g, h) in the homogeneous half-plane (left column –a, c, e, g) and PG half plane (eight column – b, d, f, h). The length of the contact area is $\boldsymbol{2b = 6}$ mm and the load is $\boldsymbol{F_n = 6}$ kN. X and Y coordinates are in mm.

Typical snapshots for spatial distributions of stress tensor components σ_x, σ_y and σ_{xy} are shown in Figure 16 for the homogeneous (left column) and PG (right column) half-planes. The distributions shown are for the contact length of $2b = 6$ mm and the total contact force $F_n = 6$ kN. The boundaries of the plastic zone are shown by a thin solid line on the corresponding snapshots. Figure 17 shows the stress components as functions of x at the depth y^* where the effective stress σ_i reaches its maximum values, namely 1 mm and 2 mm for the contact lengths of 3 mm and 6 mm, respectively. As follows

from the dependence of the effective stress σ_i on the stress tensor components, the magnitude of σ_i is influenced by the difference $(\sigma_x - \sigma_y)$ and the absolute value of the shear stress σ_{xy}. Due to the plastic zone formation the absolute values of σ_x increase (Figure 17b), while the absolute values of σ_y decrease (Figure 17c). With $|\sigma_y| > |\sigma_x|$ and same sense for both the stress components (compressive), the absolute value of their difference decreases around point $(0, y^*)$, leading to displacement of the maximum value location away from the axis of symmetry. Formation of the dumbbell-shaped region of the effective stress maxima is enhanced by a significant increase in shear stress σ_{xy} at locations further away from the axis of symmetry, reflecting the behavior of a thick beam on a compliant foundation. As can be seen from Figure 16b and 16d, a significant increase in the effective stress at the upper boundary between the elastic and plastic zones is caused by the development of a zone with tensile stress σ_x.

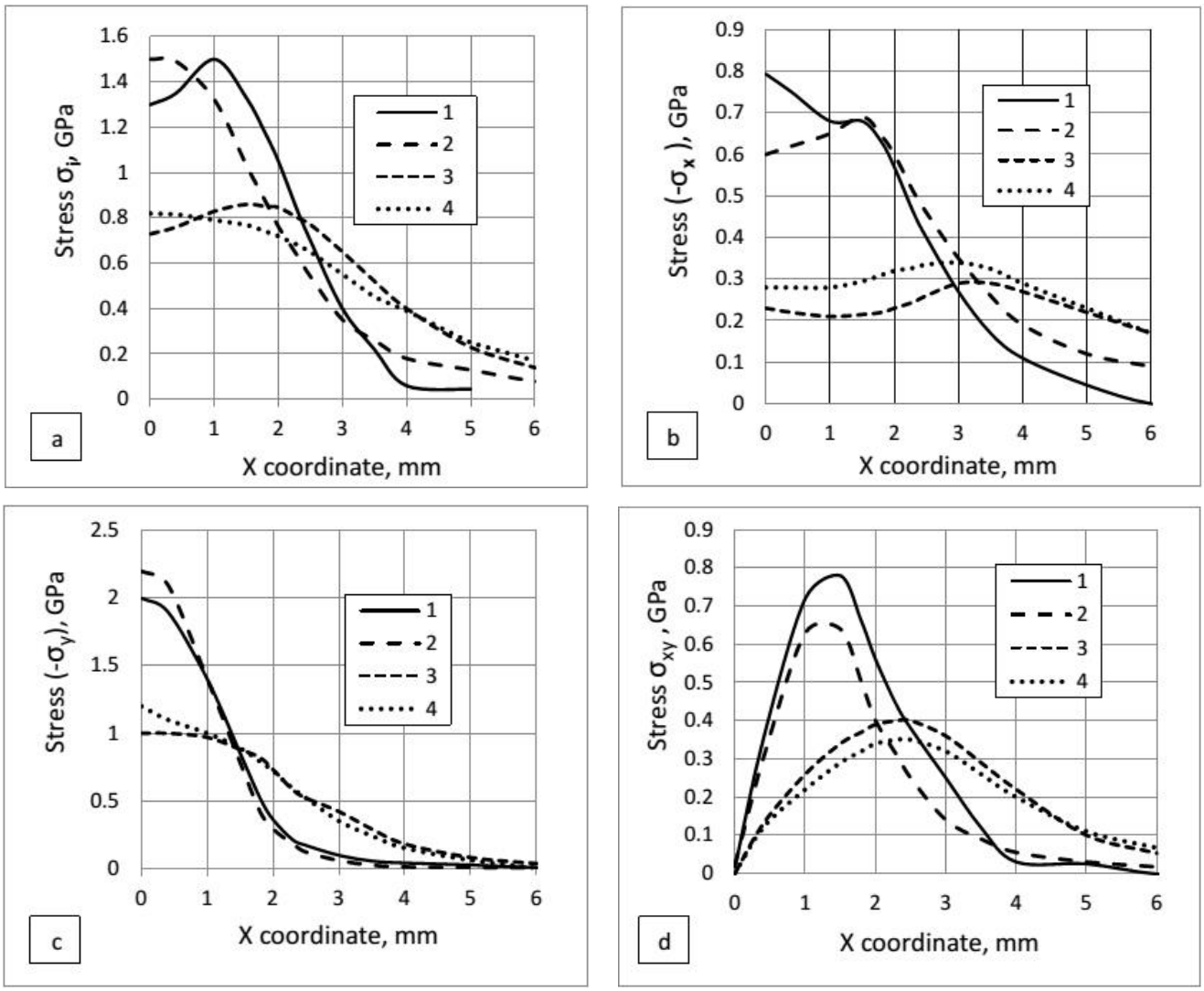

Figure 17. Stress distributions at the depth $\boldsymbol{y^*}$ of maximum effective stress: 1– PG half-plane, contact length of 3 mm, $\boldsymbol{y^* = 1}$ mm; 2 - homogeneous half-plane, contact length of 3 mm, $\boldsymbol{y^* = 1}$ mm; 3 - PG half-plane, contact length of 6 mm, $\boldsymbol{y^* = 2}$ mm; 4 - homogeneous half-plane, contact length of 6 mm, $\boldsymbol{y^* = 2}$ mm. Load $\boldsymbol{F_n = 6}$ kN.

4. Summery

The analysis presented herein indicates that surface hardened solid bodies can be treated as plastically graded with the yield strength parameter being described by a nonlinear function of depth, decreasing from a high value at the surface to a low value in the bulk of the material. It is shown both experimentally and numerically that due to a contact overloading closed-shape plastic zones form beyond the surface, where the acting stresses exceed the *local* elastic limit. The depth of the origin of plastic deformation significantly exceeds the depth at which the maximum effective stress develops in purely elastic contact conditions. Due to this spatial variation of the yield strength the plastic zones are shifted deeper towards the layers of lower values of the yield stress, while an extended narrow zone below the contact area remains in the elastic regime.

The shape, size and location of the plastic zones, determined in the experiments and numerically using the finite element method are in good agreement. The shape and size of the plastic zones as well as the distribution of the hardness increments as a result of the plastic deformation under plane strain and plane stress conditions are not fundamentally different, similar to the plane elastic problem.

It is shown that the stress fields in a PG body changes significantly with formation of a subsurface plastic zone. In the contact area two maximum appear in the distribution of effective stress σ_i, equidistant from the symmetry axis. The distance between the maxima increases with increasing the length of contact and the loading force. Tensile stress σ_x appears at a depth of the upper boundary between the elastic and plastic zones and at the free surface in the vicinity of the contact load. The maximum values of this tensile stress are most strongly dependent on the force load F_n at small contact length and high contact pressure.

The observed stress perturbations in the stress fields are of high practical importance and can significantly affect serviceability and durability of a surface hardened mechanical part. The influence of contact friction, perturbations in the distribution of the contact stresses along contact, effect of the contact surface curvatures, effect of cyclic loading and unloading on the evolution of the plastic zones and stress redistribution, including the shape, size and location of the plastic zones, and the resultant degradation of subsequent serviceability are subjects of further investigation.

References

Baker, A.J., 2012. Finite elements : computational engineering sciences. Wiley, Hoboken.

Branch, N.A., Arakere, N.K., Subhash, G., Klecka, M.A., 2011. Determination of constitutive response of plastically graded materials. International Journal of Plasticity 27, 728-738.

Choi, I., Detor, A., Schwaiger, R., Dao, M., Schuh, C., Suresh, S., 2008a. Mechanics of indentation of plastically graded materials—II: Experiments on nanocrystalline alloys with grain size gradients. Journal of the Mechanics and Physics of Solids 56, 172-183.

Choi, I.S., Dao, M., Suresh, S., 2008b. Mechanics of indentation of plastically graded materials—I: Analysis. Journal of the Mechanics and Physics of Solids 56, 157-171.

Del, G.D., 1971. Stress Determination in the Plastic Region from Hardness Distribution. Mashinostroenie, Moscow.

Devyatchenko, L.D., Tsun, A.M., Tikhonovsky, M.G., 1982 Statistical analysis of operating conditions of work rolls during cold rolling. Steel USSR 12.

Giannakopoulos, A.E., 2002. Indentation of plastically graded substrates by sharp indentors. International Journal of Solids and Structures 39, 2495-2515.

Gu, Y., Nakamura, T., Prchlik, L., Sampath, S., Wallace, J., 2003. Micro-indentation and inverse analysis to characterize elastic-plastic graded materials. Mat Sci Eng a-Struct 345, 223-233.

Johnson, K.L., 1987. Contact mechanics. Cambridge University Press, Cambridge Cambridgeshire ; New York.

Klecka, M.A., Subhash, G., Arakere, N.K., 2011. Determination of Subsurface Hardness Gradients in Plastically Graded Materials via Surface Indentation. Journal of Tribology 133, 031403-031403.

Klecka, M.A., Subhash, G., Arakere, N.K., 2013. Experimental and Numerical Modeling of Surface Indentation Response of Plastically Graded Materials. Journal of Engineering Materials and Technology 135, 041004-041004.

Moussa, C., Bartier, O., Mauvoisin, G., Pilvin, P., Delattre, G., 2012. Characterization of homogenous and plastically graded materials with spherical indentation and inverse analysis. Journal of Materials Research 27, 20-27.

Oberg, E., Jones, F.D., Horton, H.L., 1979. Machinery's Handbook. Industrial Press.

Pryor, R.W., 2012. Multiphysics modeling using COMSOL 4 : a first principles approach. Mercury Learning and Information, Dulles, Va. ; Boston, Mass.

Roberts, W.L., 1978. Cold rolling of steel. M. Dekker, New York.

Serensen, S.V., Kogaev, V.P., Shneiderovich, R.M., 1975. Bearing Capacity and Strength Calculation of Machine Parts: Handbook. Mashinostroenie, Moscow.

Suresh, S., 1997. Modeling and design of multi-layered and graded materials. Prog Mater Sci 42, 243-251.

Suresh, S., Giannakopoulos, A.E., Alcala, J., 1997. Spherical indentation of compositionally graded materials: Theory and experiments. Acta Mater 45, 1307-1321.

Thomsen, E.G., Yang, C.T., Kobayashi, S., 1965. Mechanics of plastic deformation in metal processing. Macmillan.

Tsun, A.M., 1985. Modelling of local overloadings of rolls in thin sheet rolling, PhD Dissertation, Magnitogorsk Technical University, pp. 225 (in Russian).

Williams, J.A., Dyson, I.N., Kapoor, A., 1999. Repeated loading, residual stresses, shakedown, and tribology. Journal of Materials Research 14, 1548-1559.

Yuan, F., Jiang, P., Xie, J., Wu, X., 2012. Analysis of spherical indentation of materials with plastically graded surface layer. International Journal of Solids and Structures 49, 527-536.

Zimmerman, W.B.J., 2004. Process Modelling and Simulation with Finite Element Methods. World Scientific.